6-18-2018

Fan Performance Scaling With Inlet Distortions

J. J. Defoe
University of Windsor

E. Etemadi
University of Windsor

D. K. Hall
Massachusetts Institute of Technology

Fan Performance Scaling With Inlet Distortions

J. J. Defoe*

M. Etemadi

Turbomachinery and Unsteady Flows Research Group

Department of Mechanical, Automotive, and Materials Engineering

University of Windsor

Windsor, ON N9B 3P4, Canada

e-mail: jdefoe@uwindsor.ca

D. K. Hall

Gas Turbine Laboratory

Department of Aeronautics and Astronautics

Massachusetts Institute of Technology

Cambridge, Massachusetts 02139

ABSTRACT

Applications such as boundary-layer-ingesting fans, and compressors in turboprop engines require continuous operation with distorted inflow. A low-speed axial fan with incompressible flow is studied in this paper. The objectives are to (1) identify the physical mechanisms which govern the fan response to inflow distortions and (2) determine how fan performance scales as the type and severity of inlet distortion varies at the design flow coefficient. A distributed source term approach to modeling the rotor and stator blade rows is used in numerical simulations in this paper. The model does not include viscous losses so that changes in diffusion factor are the primary focus. Distortions in stagnation pressure and temperature as well as swirl are considered. The key findings are that unless sharp pitchwise gradients in the diffusion response, strong radial flows, or very large distortion magnitudes are present, the response of the blade rows for strong distortions can be predicted by scaling up the response to a weaker distortion. In addition, the response to distortions which are composed of non-uniformities in several inlet quantities can be predicted by summing up the responses to the constituent distortions.

1 Introduction

There are many applications in which fans and low hub-to-tip radius ratio compressors must operate continuously with inlet flow distortion. Examples include boundary-layer-ingesting (BLI) fans, compressors in turboprop engines, and first compressor stages of land-based gas turbines used for power generation. The impact of individual distortion patterns on fans and compressors has been studied in the literature, particularly for BLI configurations. Some recent examples are discussed here; the list of works cited is by no means comprehensive.

Fidalgo, Hall, and Colin [1] studied NASA stage 67 subject to a 120°-sector stagnation pressure distortion both experimentally and computationally. Their computational grid was comprised of 42 million cells and the approach, directly modeling the blade rows, required unsteady computations despite the inflow and outflow boundaries not being time-dependent. The key finding was that flow redistribution upstream of the rotor enables the stage to accommodate a higher level of inlet distortion than would otherwise be possible, but that this redistribution introduces swirl into the flow, altering rotor incidence which changes the local work input.

Gunn and Hall [2] utilized a low-speed experimental fan rig to assess the impact of BLI on fan operation at cruise. The main findings were that fan efficiency was reduced by 1-2% and that a computational comparison of the low-speed fan and a transonic fan showed that the same mechanisms are responsible for changes in local blade row aerodynamics in both flow regimes. A single inlet stagnation pressure profile was considered based on work from the Cambridge-MIT Silent Aircraft Initiative [3].

Perovic, Hall, and Gunn [4] used the same experimental rig to investigate the impact of BLI on stall inception. The key finding was that the overall effect of BLI on stall margin is only 1-2% of flow coefficient. The reason is that disturbances which can lead to stall decay when they encounter regions of locally low incidence around the rotor circumference near the tip. Again in this work a single stagnation pressure distribution was used.

The response of engines to inlet stagnation temperature distortions has received less attention than that for stagnation pressure distortions, typically being only considered in applications or circumstances involving reingestion of hot exhaust gas, such as STOVL aircraft. Williams [5] gives an overview of typical inlet temperature distortion descriptors and correlation methods for engine performance response. Many studies, e.g., by NASA [6–9], have considered the impact of different inlet temperature distortions on engine performance and stability, but to the authors' knowledge, there has been no investigation into the mechanisms and distributions of increased loss in the first compressor stages.

Page, Hield, and Tucker [10] numerically investigated the impact of several inlet distortion features on transonic fan rotor stall. Three-dimensional, unsteady computations were used. The main finding was that low momentum flow must be concentrated in the tip region to have a significant impact on stall margin. Swirl and static pressure distortions were not found to be detrimental to stall margin. While several distortions were studied, for the type found to have a significant effect (tip region total pressure distortion), only a single distribution was investigated so that scaling effects could not be extracted.

Investigating the response of turbomachinery to inlet flow distortion is ordinarily time-consuming, due to the requirement to either gather experimental data or else to compute full-annulus, unsteady flow solutions. This explains why each of the above studies considered only a single inlet distortion. Doing so can provide much insight into the manner in which a fan

responds to distortion, but does not allow for assessment of the scaling of performance metrics such as efficiency as the inlet distortion details change.

On the contrary, in this paper a variety of inlet flow distortions are considered. This is achieved using a non-axisymmetric turbomachinery throughflow method recently developed by Hall, Greitzer, and Tan [11], which enables rapid assessment of fan response for a variety of non-uniform inflows. The basic idea behind the model, which dates back to Marble [12] and Horlock [13, 14], is to replace the three-dimensional blade geometry in a throughflow analysis with momentum and energy source distributions that generate the flow turning and pressure rise of the turbomachinery in a pitchwise-averaged sense. The advantage of utilizing such an approach to study the effects of inlet distortion is that the flow model is steady, avoiding the need for transient computations with their associated high cost.

Similar approaches to the one employed here have been used to assess the effects of non-uniform flow on compressor stability [15], fan stage performance due to angle-of-attack effects [16], and fan aeroacoustics [17]. Unlike these previous methods, in which the source distributions are extracted from blade passage flow field solutions for uniform inlet conditions, the sources in the approach used in this work are determined as a function of local flow conditions and an approximate blade geometry as described in Ref. [11]. This eliminates the need for a detailed blade geometry or single-passage calibration computations.

The objective of the work presented in this paper is to assess how the performance of a fan stage is affected by various types of inlet distortion at the stage design flow coefficient. The types of flow distortions considered are: (1) vertically stratified variations in stagnation pressure and (2) radial and circumferential variations in stagnation pressure, temperature, and/or swirl angle; these will be referred to as radially stratified distortions.

The key findings are that for many practical distortions (1) the response of a low-speed fan to local throughflow distortions diffusion factor to a strong distortion can be predicted by scaling up the response to a weaker distortion, and (2) that the response of a fan to distortions of several inflow quantities can often be predicted by summing the responses to the constituent distortions. These findings hold so long as neither the radial flows nor the distortion magnitude is too large. Further, inflow distortions which yield very large pitchwise gradients in the rotor or stator response are not well-predicted by scaling and summing.

The paper is organized as follows. First, the details of the fan studied and the numerical modeling approach are provided along with an introduction to the flow distortions studied. Second, physical mechanisms which govern the rotor and stator responses to inlet distortions of stagnation pressure, stagnation temperature, and swirl are described. Following this, the effects of both individual and combined distortion patterns are presented and the manner in which the changes scale is assessed.

2 Approach

2.1 Whittle Laboratory Low Speed BLI Fan Rig

The computations are carried out for the fan rig geometry used at the Whittle Laboratory in Refs. [2,4,18]. A meridional view of the stage geometry as modeled in the computations is given in Fig. 1. The figure also indicates the location of axial

measurement planes from which computational results will be shown. The inflow and outflow boundaries are located approximately two diameters upstream of the spinner tip and downstream of the stator trailing edge, respectively. Approximate blade row camber angle distributions were estimated based on radial distributions of leading and trailing edge metal angles. Table 1 lists the relevant design parameters of the fan rig. All results in this work were calculated at the design point flow coefficient.

2.2 Non-Axisymmetric Throughflow Analysis

To reduce the computational cost of investigating the effects of many inlet distortions to a manageable level, the source term approach of Hall, Greitzer, and Tan [11] is used to model the fan blade rows. The model does not include viscous losses so Euler computations are used. Distortion transfer is well-captured by the approach for flows for which the local rotor reduced frequency,

$$f_{\mathrm{red}} = \frac{c_x/V_x}{2\pi/\Omega} \approx \frac{\cos\xi\,(1 - R_{\mathrm{hub}}/R_{\mathrm{tip}})}{2\pi\phi(\mathrm{AR})} \tag{1}$$

is small, $f_{\mathrm{red}} \ll 1$. Here c_x is the axial chord, V_x is the axial velocity, Ω is the angular velocity, ξ is the blade stagger angle, ϕ is the local flow coefficient, AR is the blade aspect ratio, and R_{hub} and R_{tip} are the hub and tip radii, respectively. For the fan stage and distortions considered in this paper, $f_{\mathrm{red}} < 0.1$ over the full span at design.

Ansys CFX 14 [19] is used to carry out the computations. As CFX does not explicitly contain an inviscid solver, laminar flow with zero-viscosity air and slip walls are used to compute effectively inviscid flow solutions.

The computational domain consists of the full annulus of the fan including extended inlet and outlet ducts as depicted in Fig. 1. The total grid count is 2.6 million cells using a fully structured hexahedral mesh created using Pointwise [20]. Note that compared to the computations in Gunn and Hall [2], this represents a 30-fold decrease in grid count. In addition, the computations in the present work are steady. Thus the total computational cost reduction compared to unsteady, full-wheel computations in which all boundary layers are resolved is approximately 2-3 orders of magnitude.

Grid independence was assured by studying several grid levels; the selected grid was the second of four levels—the coarsest at which no further changes in design loading coefficient were obtained with grid refinement. The slope of the characteristic was unchanged for all grid levels.

2.3 Inlet Distortions

Two types of distortions are considered: vertically-stratified and radially-stratified.

2.3.1 Vertically Stratified Distortions

These distortions of inlet stagnation pressure emulate those caused by BLI-type propulsor integration with an airframe. The distortions are defined in terms of a normalized difference between maximum and minimum stagnation pressure,

$\Delta p_t/\overline{\rho}_1^M U_{\rm mid}^2$. The variation in stagnation pressure is set to yield a quadratic velocity profile, and the values of $\Delta p_t/\overline{\rho}_1^M U_{\rm mid}^2$ are representative of low-speed turbulent boundary layers. The fraction of the inlet duct diameter over which the stagnation pressure varies from minimum to maximum, $\delta/2R_{\rm in}$ (where δ is the thickness of the boundary layer giving rise to the distortion and the inlet duct radius is $R_{\rm in}$) is also varied. Figure 2 schematically illustrates the imposed distortion at the duct inlet. Also shown is the direction of rotor rotation and the location of $\theta = 0$. The specific combinations of the two parameters considered are indicated in the upper part of Tab. 2.

2.3.2 Radially Stratified Distortions

These distortions of inlet stagnation pressure, stagnation enthalpy, and swirl emulate those seen by the first compressor stage of a turboprop engine. In these engines, the propeller is typically rotating about an axis offset from the engine core axis. Though a fan is used in the current work, the hub-to-tip radius ratio of first stage compressors in such engines can be as low as 0.5 [21] so radial effects are still important. Therefore the qualitative effects of distortion for the fan stage are not expected to be dramatically different than those which would be seen in such compressors. The distortions are defined relative to the axis of rotation of the hypothetical upstream propeller; primed quantities are defined relative to that axis. Two parameters describe the radially stratified distortions. One is the amount of swirl imparted by the upstream propleller α'; this is uniform relative to the propeller axis but yields non-uniform inlet swirl relative to the fan axis. The amount of swirl also determines the radial gradient of stagnation enthalpy, dh_t/dr', in conjunction with the flow coefficient and an assumed rotational speed for the hypothetical propeller via the Euler turbine equation. The propeller is assumed to be isentropic so that, for low-speed flow,

$$\frac{dh_t}{dr'} = \frac{1}{\overline{\rho}_1^M}\frac{dp_t}{dr'}. \tag{2}$$

Both co-swirl (same direction as rotor rotation, $\alpha' > 0$) and counter-swirl (opposite direction of rotor rotation, $\alpha' < 0$) are considered. The other parameter is the offset between the fan axis and the propeller axis, ΔR. The parameters are illustrated schematically in Fig. 3. All radial distortions studied are consistent with this figure; the rotor rotation direction and $\theta = 0$ location are again shown. The specific combinations used are indicated in Tab. 2; cases with no swirl or with swirl but no variation in h_t/p_t are included to assess the effects of these inflow non-uniformities individually.

2.4 Diffusion Factor

The source term description of the fan blade row is inviscid, so the impact of the distortions on fan efficiency cannot be directly assessed. Instead, diffusion factor is used as a proxy for blade performance. The local diffusion factor is

approximated as

$$D = 1 - \frac{W_{\rm out}}{W_{\rm in}} + \frac{1}{2}\frac{|r_{\rm out}W_{\theta{\rm out}} - r_{\rm in}W_{\theta{\rm in}}|}{W_{\rm in}}\frac{2\pi/B}{c_{\rm ref}}, \tag{3}$$

where W is the relative velocity (equal to the absoluate velocity, V, in the stator), $r_{\rm in}$ and $r_{\rm out}$ are respectively the local streamtube radius at the measurement plane upstream and downstream of the blade row, N is the number of blades, and $c_{\rm ref}$ is the midspan meridional chord of each blade row. The focus is on relative variation in D so this level of approximation is acceptable. It has been shown that the mechanisms governing distortion response are inviscid, and that efficiency changes track with diffusion factor changes [2]. Higher local diffusion than for uniform flow indicates a likely increase in local entropy generation and thus a contribution to reduced overall efficiency. Both increases in diffusion and circumferential distortions in diffusion are thought to decrease efficiency. We therefore consider circumferential variation in diffusion factor relative to the pitchwise average,

$$\Delta D = D - \overline{D}^{\theta}, \tag{4}$$

as a measure of increased loss due to inlet distortion relative to performance with uniform flow.

3 Distortion Response Mechanisms

In this section, we describe the physical mechanisms of fan stage response to stagnation pressure, stagnation temepra-ture/enthalpy, and swirl distortions. The response is described in terms of (i) upstream flow redistribution, (ii) non-uniform stagnation enthalpy rise, stagnation pressure rise, and streamtube contraction through the fan rotor, i.e., *distortion transfer*, and (iii) stator response to rotor exit distortion. The details of each of these processes differs depending on the type of inlet distortion, but this decomposition provides insight into the mechanisms that drive the scaling of the response to different distortions considered in Section 4.

3.1 Rotor Stagnation Pressure Distortion Response

The fan rotor response to an offset radial stagnation pressure distortion is illustrated in Fig. 4. Figure 4(a) shows the rotor incidence, calculated as the difference between the local blade-relative flow angle and its circumferential average at a given radius. The incidence is high near $\theta = 0$ for tip and midspan sections due to the presence of low stagnation pressure (labeled A in Fig. 4). The low stagnation pressure flow is accelerated more strongly than the high stagnation pressure flow near the left side of the wheel, resulting in a left-to-right flow redistribution. This causes counter-swirl and increased incidence on one side of the hub (at B), and co-swirl and decreased incidence on the other (at C). A consequence of the fan-distortion interaction is that the incidence distortion is largest near the hub, due to the upstream redistribution, rather than near midspan

where the inlet stagnation pressure distortion is largest.

The rotor distortion transfer can be characterized in terms of the non-uniform work input and streamtube contraction through the rotor, illustrated in Fig. 4(b) and 4(c). Increased incidence leads to increased flow turning, and the non-uniformity in stangation enthalpy rise is similar to that in incidence, with high loading near $\theta = 0$ and near the hub as the rotor exits the low stagnation pressure region, and low loading on the opposite side of the hub as the rotor enters the low stagnation pressure region. The non-uniform work input leads to non-uniform streamtube contraction, with larger relative increases in axial velocity across the rotor with increased work input, particularly at the hub near $\theta = 0$ (at D).

Circumferential non-uniformities in rotor diffusion factor, shown in Fig. 4(d), result from the combination of non-uniform flow turning and streamtube contraction. The largest increase in diffusion factor occurs near the tip (at E) where the increase in stagnation enthalpy rise is also largest. The largest *decrease* in diffusion factor (relative to the circumferential average) occurs near the right side of the hub (at F), due to larger streamtube contraction, even though the incidence and enthalpy rise are relatively high. The significant differences between the shape of the inlet distortion and the rotor diffusion factor distribution (indicative of local blade performance) illustrates the importance of fan-distortion interaction and upstream flow redistribution in low hub-to-tip ratio machines.

In summary, the mechanisms of rotor stagnation pressure distortion response are (i) upstream flow redistribution from regions of high stagnation pressure to low stagnation pressure, yielding non-uniform (ii) rotor incidence distribution, (iii) rotor stagnation enthalpy rise, and (iv) rotor streamtube contraction. Distortions in rotor diffusion factor are driven by the latter two of these effects, with increase stagnation enthalpy rise (i.e., flow turning) increasing local diffusion and increased streamtube contraction alleviating it. While the details of the redistribution and distortion response vary with the shape and intensity of the inlet distortion, these mechanisms describe the dominant effects for the range of offset radial distortion considered here, and similar effects have been previously reported for vertically stratified BLI-type inlet stagnation pressure distortions [2, 11].

3.2 Rotor Stagnation Temperature Distortion Response

For incompressible flow, the streamline pattern through the stage is unaffected by inlet stagnation temperature non-uniformity, and the changes in swirl angle through the rotor and thus the stagnation enthalpy rise are uniform. This is illustrated in Fig. 5(a), which shows the shape of the radial-offset inlet distortion has been preserved through rotor with a uniform increase in stagnation temperature and variation in the shape of the distribution due to the swirl imparted by the rotor. The main effect of the temperature distortion on rotor performance is to introduce a density non-uniformity, which, coupled with the uniform stagnation enthalpy rise, results in non-uniform stagnation pressure rise through the rotor, shown in Fig. 5(b). This leads to a non-uniformity in diffusion, with increased de Haller number (ratio of relative velocities exiting and entering the rotor), shown in Fig 5(c), and decreased diffusion factor, shown in Fig 5(d) where the incoming stagnation temperature is low.

Two observations about the applicability of this analysis must be made here. The first is that it has been carried out for incompressible flow, which decouples the stagnation temperature distribution from the streamline pattern through the stage;

for transonic flows representative of fans and low pressure compressor stages, further analysis including the coupling between the dynamics and thermodynamics at higher Mach numbers is required. The second observation is that the magnitude of the temperature distortion considered here is much larger than would be generated by an upstream propeller with the stagnation pressure distortion described above; this was done intentionally to magnify the effect of the distortion response to be identified. For the type of distortions considered in this paper, due to boundary layer ingestion and upstream propellers, it is expected that the stagnation pressure distortion effects described above and the swirl distortion effects described below will have a stronger affect on turboamchinery performance than stagnation temperature distortions.

3.3 Rotor Inlet Swirl Distortion Response

The main impact of inlet swirl distortion on the rotor is through distortions in rotor incidence. Parts (a) and (b) of Fig. 6 show the rotor-relative swirl angle at stations 1 and 2, illustrating the propagation of the inlet vortex, which starts at $\theta = 0$ at the inlet, and self propogates clockwise a quarter of the way around the annulus ahead of the rotor leading edge. The localized clockwise swirl results in regions of counter-swirl at the hub near the vortex core (at A), and co-swirl at the casing (at B) and on the hub on the opposite side (at C). As for the inlet stagnation pressure distortion, distortions in rotor stagnation enthalpy rise and streamtube contraction, shown in parts (c) and (d) of Fig. 6, are similar to the incidence distortion.

Figure 6(e) and Fig. 6(f) show similar patterns in rotor de Haller number and diffusion factor distortions. The combined effect of incidence and streamtube contraction distortions yield a region of increased diffusion across the entire span (at D) and a localized region of decreased diffusion where the streamtube contraction is low (at E). Examination of the response of different swirl distortions listed in Table 2 shows the dominant factors and thus the shape of the diffusion factor distortion change with swirl intensity and radial location, but can always be explained in terms of the combined incidence, loading, and streamtube contraction non-uniformities.

3.4 Stator Response to Rotor Exit Distortion

Figure 7 shows distortions in rotor exit axial velocity and stator diffusion factor for the three inlet distortions considered above. In all cases, the diffusion factor is highest where the axial velocity into the stator is lowest. Since there is no work input in the stator, the stator diffusion factor is driven by non-uniformities in stator inlet swirl angle, with higher values where the inlet swirl, and thus velocity reduction and circulation change through the stator, are largest.

The dependence on rotor exit axial velocity is illustrated schematically in Fig. 8, which shows stator velocity triangles for two different axial velocities. For uniform rotor-relative exit flow angle, β_3, an increase in local axial velocity leads to a decrease in local absolute swirl angle α_3, and thus in stator circulation change and diffusion factor.

4 Distortion Response Scaling

In this section, the response of the fan to the inlet flow distortions listed in Table 2 are presented and discussed.

4.1 Vertically Stratified Stagnation Pressure Distortion

The impact of the distortion extent is discussed first, followed by the impact of the distortion magnitude.

4.1.1 Distortion Extent

The maximum variation in diffusion caused by vertically stratified stagnation pressure distortions increases with $\delta/2R_{in}$ in both the rotor and stator, but the marginal increases are reduced as $\delta/2R_{in}$ increases and for $\delta/2R_{in} \geq 0.75$ the maximum diffusion saturates across the span as can be seen in Fig. 9. Rotor input variations saturate in a similar manner. The reason for this behavior is that changing $\delta/2R_{in}$ changes the circumferential and radial distribution of the non-uniform inlet conditions. Circumferential non-uniformities at a given radius may therefore change, even though the overall distortion magnitude does not. The nature of the coordinate transformation between vertically stratified flow conditions for an axisymmetric machine leads to the observed non-linear flow behavior.

4.1.2 Distortion Magnitude

In Fig. 10, the variations in diffusion factor for the three values of $\Delta p_t/\overline{\rho}_1^M U_{\text{mid}}^2$ used (0.055, 0.094, and 0.117) are given in gray. The impact of the weakest distortion is scaled up linearly and this is also shown in the figure; the scaling factor for the solid black curve is $0.094/0.055 = 1.71$ while for the dashed black curve it is $0.117/0.055 = 2.13$.

Scaling up by a factor of 1.71 predicts the behavior of the distortion with $\Delta p_t/\overline{\rho}_1^M U_{\text{mid}}^2 = 0.094$ well overall. The normalized RMS error, defined as

$$\hat{e}_{\text{RMS}} = \frac{e_{\text{RMS}}}{\left(\Delta D\left(\theta\right)_{\max} - \Delta D\left(\theta\right)_{\min}\right)_{\text{actual}}}, \tag{5}$$

where

$$e_{\text{RMS}} = \sqrt{\frac{1}{2\pi}\int_{\theta=0}^{\theta=2\pi}\left(\left(\Delta D\right)_{\text{predicted}} - \left(\Delta D\right)_{\text{actual}}\right)\right)^2 d\theta}, \tag{6}$$

is 6.5%, 4.2%, and 11.0% in the rotor at 10%, 50%, and 90% span, respectively. In the stator at these three spanwise locations $\hat{e}_{\text{RMS}} = 6.2\%$, 6.2%, and 7.7%. Scaling up by 2.13 times predicts the behavior for the strongest distortion less well, yeilding $\hat{e}_{\text{RMS}} =$ between 7% and 21% in the rotor and between 12% and 15% in the stator. Qualitatively the effect of increasing distortion magnitude is seen to be to scale up the rotor diffusion non-uniformity response. The scaling is nearly linear for small distortion magnitudes, while for larger distortion magnitudes linear scaling captures the overall shape of the response but yields significant over-prediction. The linear scaling can be explained by the fact that varying the distortion magnitude does not alter the "shape" of the incoming flow field. Thus knowing the response of the fan to a distortion of one magnitude can allow for an approximate prediction of the response for other magnitudes by scaling linearly. The

approximation becomes less accurate as the distortion magnitude increases because of the non-linear relationship between $\Delta p_t/\overline{\rho}_1^M U_{\mathrm{mid}}^2$ and the velocity triangles.

4.2 Radially Stratified Distortion without Swirl

The impact of the propeller offset is discussed first, followed by the effects of the distortion magnitude.

4.2.1 Offset Between Fan and Propeller Axes

The rotor diffusion factor does not behave linearly when scaled with the offset $\Delta R/R_{\mathrm{in}}$ except in the outermost span ($\hat{e}_{\mathrm{RMS}} \leq 11\%$). This can be seen in Fig. 11, which depicts the results of varying the offset while keeping the magnitude of the stagnation pressure and temperature (enthalpy) distortion constant at $(dh_t/dr')\left(R_{\mathrm{in}}/U_{\mathrm{mid}}^2\right) = (dp_t/dr')\left(R_{\mathrm{in}}/\overline{\rho}_1^M U_{\mathrm{mid}}^2\right) = 1.85$. This is expected as the nature of the flow field changes significantly with offset, while at the casing the flow direction is forced to satisfy the flow tangency boundary condition, limiting the ability of the imposed inflow to affect the rotor incidence angles near the casing. At zero offset the inflow is axisymmetric, while in the limit of the offset tending towards infinity the inlet flow field becomes nearly constant. In between, the maximum non-uniformity in rotor diffusion factor variation occurs at $\Delta R/R_{\mathrm{in}} = 1.00$, but like with varying the depth of vertically stratified distortions, marginal increases reduce as offset increases so that the response is generaly non-linear. In the stator, however, the region of linear behavior extends from the casing to midspan ($\hat{e}_{\mathrm{RMS}} \leq 10\%$). The enlarged region of linear behavior in the stator may be related to the significant radial flows being confined to near the hub (due to the contracting hub curve shown in Fig. 1).

4.2.2 Stagnation Enthalpy and Stagnation Pressure Distortion Magnitude

The distortions investigated with only variations in stagnation enthalpy yield nearly zero circumferential variation in diffusion factor because of the small magnitudes of distortion imposed by the isentropic propeller constraint ($(dh_t/dr')\left(R_{\mathrm{in}}/U_{\mathrm{mid}}^2\right) = 2.81$), compared to the distortion used in Section 3 which is 6.5 times stronger.

As a result of the stagnation enthalpy variations being negligible, the response of the fan for the radially-stratified stagnation pressure alone distortions and for the distortions with both p_t and h_t varying are identical and the latter are shown in Fig. 12. The figure also includes additional curves in which linear scaling based on $(dh_t/dr')\left(R_{\mathrm{in}}/U_{\mathrm{mid}}^2\right)$ is applied to the weakest distortion to match the two stronger distortions. This scaling predicts the response for the stronger distortions with $\hat{e}_{\mathrm{RMS}} \leq 8\%$ except for the $(dh_t/dr')\left(R_{\mathrm{in}}/U_{\mathrm{mid}}^2\right) = 2.81$ prediction in the rotor at 10% span (where $\hat{e}_{\mathrm{RMS}} = 36\%$). This is similar behavior to what is seen for vertically-stratified distortion though owing to the different distribution of inlet stagnation quantities the location of non-linear scaling moves from the tip (vertically-stratified) to the hub (radially-stratified). This is due to the fact that the gradients of the inlet stagnation pressure are higher near the hub than near the casing for radial stratification with $\Delta R/R_{\mathrm{in}} = 0.75$.

4.3 Radially Stratified Distortion with Swirl

Next we consider radially stratified distortions with swirl, beginning with swirl-alone distortions, and then considering combined distortions of swirl with stagnation pressure and enthalpy. With the introduction of swirl into the inflow, the angular momentum of the fluid leads to circumferential migration (orbiting) of the incoming flow field upstream of the rotor. This introduces θ (phase) shifts in the fan response depending on the magnitude and direction of incoming swirl. Thus, it is expected that the normalized RMS error $\hat{e}_{\mathrm{RMS}}$ will be in general large when assessing linear scaling. Since it is typically the most severe variations from the pitchwise-average that is of most concern for turbomachinery design, here we introduce two additional metrics for assessing the scaling behavior of distortions with swirl. These are the normalized errors in the prediction of the maximum increase in diffusion and the maximum decrease in diffusion. These are defined as

$$\hat{e}_{\max} = \frac{e_{\max}}{\left(\Delta D\left(\theta\right)_{\max} - \Delta D\left(\theta\right)_{\min}\right)_{\mathrm{actual}}}, \tag{7}$$

and

$$\hat{e}_{\min} = \frac{e_{\min}}{\left(\Delta D\left(\theta\right)_{\max} - \Delta D\left(\theta\right)_{\min}\right)_{\mathrm{actual}}}, \tag{8}$$

where $e_{\max}$ and $e_{\min}$ are the differences between the predicted and actual maximum and minimum ΔD, respectively.

4.3.1 Swirl-Alone: Magnitude Variation

With swirl-alone distortion, the inlet stagnation quantities are constant. First consider co-swirl (rotation in the same direction as the fan rotor). As can be seen in Fig. 13, the variations in diffusion factor never behave linearly in terms of addition/scaling ($19\% \leq \hat{e}_{\mathrm{RMS}} \leq 41\%$), but the maximum increase and decrease in diffusion can be approximately predicted for stronger distortions by scaling up the weaker distortions. This breaks down as the swirl angle becomes large enough that small angle approximations no longer hold ($> 10°$). For the rotor, the $10°$ co-swirl distortion's maximum increase and decrease is predicted by scaling up the $5.3°$ response with $\hat{e}_{\max} \leq 14\%$ and $|\hat{e}_{\min}| \leq 12\%$. In the stator, $\hat{e}_{\max} \leq 9\%$ but at midspan $|\hat{e}_{\min}| = 63\%$. This is because the highly localized decrease around $\theta/2\pi = 0.1$ for $5.3°$ co-swirl does not occur for higher swirl values. Near the hub and casing, the $\hat{e}_{\min}$ behavior is approximately linear ($|\hat{e}_{\min}| \leq 15\%$). In contrast, scaling up to $15°$ co-swirl, the maximum increases in diffusion are in general poorly predicted. The exception is at 10% span, where in the rotor $\hat{e}_{\max} = 11\%$ and in the stator $\hat{e}_{\max} = 3.5\%$, but the maximum increases here are small compared to diffusion factor variations at higher span fractions. Turning to the prediction of the largest decrease in diffusion, linear scaling only yields accurate results ($|\hat{e}_{\min}| \leq 4\%$) at 90% span for both rotor and stator. This is for the same reason that the 10% span maximum increase is well-predicted: the actual minima of ΔD are near zero. Linearly scaling up the response to $5.3°$ co-swirl to predict the response to $15°$ fails to capture the amplitude of the most significant variations in diffusion

factor.

Next consider counter-swirl (rotation in the opposite direction as the fan rotor). Either direction of incoming swirl is possible since the hypothetical upstream propeller giving rise to the distortion can rotate in either direction to impart the same work input to the flow. Scaling up the 5.3° counter-swirl response to predict that for 10° counter-swirl accurately captures the maximum increase in diffusion ($\hat{e}_{\max} \leq 5.4\%$) with the exception of in the rotor at 10% span ($\hat{e}_{\max} = 18\%$), but due to the small overall changes near the hub the response can be said to scale linearly. The detailed results are given in Fig. 14. The same behavior is seen for the decreases in diffusion. As with co-swirl, the scaling behavior is not as straightforward when moving to 15° counter-swirl. In the rotor $|\hat{e}_{\max}| \leq 10\%$ except at 10% span where the large spike in increased diffusion is not captured, yielding $\hat{e}_{\max} = -60\%$. The minimum diffusion is well-predicted in the rotor ($\hat{e}_{\min} \leq 13\%$). The opposite is true for the stator, with the maximum diffusion increase well-predicted ($|\hat{e}_{\max}| \leq 7.5\%$) but the minimum diffusion poorly predicted ($|\hat{e}_{\max}| \geq 56\%$) except at 90% span where $\hat{e}_{\min} = -9.1\%$. This is the only location where a large spike of decreased diffusion does not occur; such spikes are unable to be captured by linearly scaling up distortion response from lower amounts of counter-swirl.

4.3.2 Swirl Combined with Stagnation Enthalpy and Pressure Distortion: Magnitude Variation

Swirl distortion produced by an upstream propeller has a stagnation pressure/enthalpy variation associated with the swirl. Such distortions are considered here. These distortions proved too strong for the turbomachinery to deal with in some cases, resulting in localized regions of reversed flow in the rotor. The results from these cases (10° co- and counter-swirl and 15° counter-swirl) are not included in the discussion which follows as they do not represent conditions at which the fan could realistically operate.

For co-swirl, the 5.3° distortion response is scaled up to by 2.83 times. As can be seen in Fig. 15, the same phase shifts for differing amounts of swirl occur as a result of differing orbit rates as are seen for swirl-alone distortions. Therefore $\hat{e}_{\max}$ and $\hat{e}_{\min}$ are again the useful metrics to assess the behavior of the scaling response. $\hat{e}_{\max}$ is under-predicted by scaling up the weaker distortion by 25% in the rotor at 10% span while the under-prediction is $\leq 1\%$ at 50% and 90% span. This is due to the fact that the impact of radial flow varies significantly across the span due to the contracting hub profile. At the hub the mean radial flow angle is $\approx 22^\circ$ while it is less than 10° at 50% and 90% span. As a result, even though radial flow angle distortion does not vary strongly across the span, the circumferential decreases have a large impact on de Haller number distortion (which dominates the diffusion factor increase) near the hub for $\alpha' = 15.0^\circ$. This effect does not scale up accurately because of the nonlinearity of the contribution of the radial flow to $|W|$ for large angles. In contrast, scaling up the 5.3° response predicts the largest decrease in diffusion in the rotor across the span to within 13% because the radial flow angle increases do not dominate the de Haller number distortion. In the stator, the scaled response is a good predictor across the span ($|\hat{e}_{\max}| \leq 12\%$) as the main mechanism driving the stator diffusion factor response is incidence distortion as discussed in Section 3.4 and the maximum increase in incidence scales approximately linearly. The maximum decreases in diffusion factor are also reasonably well-captured by scaling in the stator, with $|\hat{e}_{\min}| \leq 15\%$ except at 50% span where $\hat{e}_{\min} = 17\%$.

The final aspect of distortion scaling assessed is whether the turbomachine response to distortions of combined swirl, stagnation enthalpy, and stagnation pressure distortion can be predicted by summing the responses to the constituent distortions. Recall from Section 4.2.2 that the stagnation enthalpy distortion alone yields insignificant variations in diffusion factor. Thus, the additive scaling behavior can be assessed by examining combinations of h_t and p_t distortion, swirl-alone distortion, and the combination of the two which was discussed earlier in this section. This is done for both co-swirl and counter-swirl. Only 5.3° is considered for the same reasons the linear scaling analysis above was limited. Recall that 5.3° corresponds to $(dh_t/dr')\left(R_{\rm in}/U^2_{\rm mid}\right) = (dp_t/dr')\left(R_{\rm in}/\overline{\rho}^M_1 U^2_{\rm mid}\right) = 0.974$. While only the inflows with swirl orbit the fan axis upstream of the rotor, due to the small swirl angle considered the associated phase shift is small. As a result, $\hat{e}_{\rm RMS}$ is a useful metric for assessing the accuracy of the additive behavior along with $\hat{e}_{\rm max}$ and $\hat{e}_{\rm min}$.

The variations in diffusion factor for the constituent distortions, their sum, and the combined distortion for the case of co-swirl are shown in Fig. 16. Overall the summation of the responses of the constituent distortions is a good predictor of the response to the combined distortion. In the rotor, $4\% \leq \hat{e}_{\rm RMS} \leq 7\%$ while in the stator $2\% \leq \hat{e}_{\rm RMS} \leq 10\%$. The maximum increases and decreases are also well-predicted in general; only $\hat{e}_{\rm min}$ in the stator at 10% span is poorly predicted (-20%). This additive behavior is remarkable considering that the circumferential distribution of the variations in diffusion factor are completely different for the combined h_t and p_t distortion and for the co-swirl alone distortion. This is most clearly illustrated in the stator at 90% span (lower right of Fig. 16); the maximum increase in diffusion for the combined h_t and p_t distortion is approximately co-located with the maximum decrease in diffusion for the co-swirl distortion. Nevertheless the combined distortion response is well-predicted by summing the responses of the constituent distortions.

The diffusion factor variations for the similar case, but with counter-swirl, are given in Fig. 17. Here the additive behavior is less apparent: while for the most part $\hat{e}_{\rm RMS} \leq 10\%$, at 10% span in the rotor $\hat{e}_{\rm RMS} = 16\%$ due to the fact that the sharp increase in diffusion for the swirl-alone distortion around $\theta/2\pi = 0.85$ is mitigated by the presence of varying inlet stagnation quantities. $|\hat{e}_{\rm max}| \leq 12\%$ except at midspan in the stator (18%). That poorer additivity is also due to the local spike in diffusion for co-swirl alone not occurring in the combined distortion. $|\hat{e}_{\rm min}| \leq 11\%$ across the span for both blade rows with the exception of the rotor at 90% span (-30%) and again this is due to a local (downward) spike in the swirl-alone distortion response being mitigated by the addition of the associated h_t and p_t non-uniformity.

5 Summary and Conclusions

In this paper, a source-term-based blade row model was used to numerically investigate the physical mechanisms by which inlet distortions of different quantities interact with a low-speed fan, and to assess the scaling of the impact of inlet flow distortion. The model does not include viscous effects so Euler computations were used. All computations were carried out at the design flow coefficient.

The key mechanism driving variations in rotor diffusion factor for practical distortions in low-speed fans is incidence variation. These may arise directly from the inlet distortion (associated with swirl or axial velocity variations due to stagnation pressure distortion) or be a result of non-uniform rotor suction (as with hub incidence swings when stagnation pressure varies). Incidence variations give rise to non-uniform work input (increases diffusion factor) and streamtube contraction

(decreases diffusion factor). Stagnation temperature variations result in density distortion which leads to non-uniform stagnation pressure rise and thus de Haller number and diffusion factor distortions. These effects tend to be small for temperature variations consistent with boundary layer ingestion or upstream propellers. For other conditions such as re-ingestion of hot gas from thrust reversers, these effects may be significant.

The stator diffusion factor response is primarily driven by axial velocity non-uniformities via changes to the velocity triangles and stator incidence, where low axial velocity yields increased diffusion factor and vice-versa.

The behavior of the fan diffusion factor response scales linearly (less than 15% normalized error) in many cases because for low-speed flow practical distortions generally involve small perturbations in the inlet quantities. The strongest distortions considered are generally less well-predicted by scaling up weaker distortions because the perturbations are no longer small. The extent of vertically stratified distortions yields a highly non-linear response due to the fact that in polar coordinates the "shape" of the distortion changes significantly with extent. For radially stratified distortions without swirl, the fan diffusion factor response behaves in a linear manner except in regions where strong radial flows can exist. For swirl alone distortions the fan response can be scaled up so long as the incoming perturbations are small, except where very high spatial gradients of diffusion factor variation occur. For distortions with these high gradients in the fan response, scaling up does not yield a useful prediction of the response to a stronger distortion. When swirl is combined with variations in inlet stagnation quantities, the response to stronger distortions can be predicted by scaling up except, again, where radial flows are significant. The response of the fan to combined distortions of swirl and stagnation quantities can be predicted by combining the responses to the constituent distortions except where the swirl-alone distortions produce high gradients in diffusion factor variation. These gradients are reduced when stagnation quantities also vary due to flow redistribution.

The key findings are that (1) in many cases the response of fan diffusion factor to a strong distortion can be predicted by scaling up the response to a weaker distortion, and (2) that the response of a fan to distortions of several inflow quantities can often be predicted by summing the responses to the constituent distortions. This can be done so long as (1) radial flows are not too large a contributor to the overall (relative) velocity, (2) the distortion magnitude is not too large, and (3) the distortion responses do not involve very large pitchwise gradients of diffusion factor.

Future work should include viscous forces in the fan model to directly enable the prediction of efficiency changes resulting from inlet distortions. The development of such a general viscous model is non-trivial. In addition, a high-speed fan should be considered to assess the impact of Mach number on the findings reported here. The qualitative behavior is expected to be the same [2] but the quantitative results will almost certainly change.

Acknowledgements

The authors would like to acknowledge E. J. Gunn, D. Perovic, and C. A. Hall of the Whittle Laboratory for information about their test rig. Computational resources were provided by the facilities of the Shared Hierarchical Academic Research Computing Network (SHARCNET: www.sharcnet.ca) and Compute/Calcul Canada.

Nomenclature

$A =$ area

AR $=$ blade aspect ratio

$B =$ number of blades

$c =$ chord length

$e =$ diffusion factor distortion error metric

$\hat{e} =$ normalized diffusion factor distortion error

$D =$ diffusion factor

$f_{\mathrm{red}} =$ reduced frequency

$h =$ enthalpy

$\dot{m} =$ mass flow rate

$M =$ Mach number

$p =$ pressure

$r =$ radial coordinate

$R =$ radius

$T =$ temperature

$U =$ rotor blade speed

$V =$ velocity in stationary frame

$W =$ velocity in rotating frame

$y =$ vertical coordinate

$\alpha =$ absolute flow angle

$\beta =$ relative flow angle

$\delta =$ boundary layer thickness

$\Delta D =$ change in diffusion factor

$\Delta R =$ offset between fan axis and center of distortion pattern

$\theta =$ circumferential coordinate

$\rho =$ density

$\phi =$ flow coefficient ($\dot{m}/(\bar{\rho}^M A_1 U_{\mathrm{mid}})$)

$\xi =$ blade stagger angle

$\Omega =$ rotor angular velocity

Subscripts

des = design

in = inlet

mid = 50% span value

min = minimum

max = maximum

out = outlet

ref = reference value

t = stagnation

x = axial component

1–4 = measurement plane locations

∞ = free-stream quantity

θ = tangential component

Superscripts

M = mass-weighted average quantity

θ = circumferential average quantity

References

[1] Fidalgo, V. J., Hall, C. A., and Colin, Y., 2012, "A Study of Fan-Distortion Interaction Within the NASA Rotor 67 Transonic Stage," ASME J. Turbomach., **134**(5), p. 051011.

[2] Gunn, E. J., and Hall, C. A., 2014, "Aerodynamics of Boundary Layer Ingesting Fans," ASME Paper No. GT2014-26142.

[3] Madani, V., and Hynes, T., 2009, "Boundary Layer Ingesting Intakes: Design and Optimization," *19th International Society for Air Breathing Engines Conference, Montreal, Canada*.

[4] Perovic, D., Hall, C. A., and Gunn, E. J., 2015, "Stall Inception in a Boundary Layer Ingesting Fan," ASME Paper No. GT2015-43025.

[5] Williams, D. D., 1986, "Review of Current Knowledge on Engine Response to Distorted Inflow Conditions," *Engine Response to Distorted Inflow Conditions* (AGARD Conference Proceedings, No. 400), Advisory Group for Aerospace Research and Development, Neuilly sur Seine, France.

[6] Braithwaite, W. M., Graber, E. J., and Mehalic, C. M., 1973, "The Effects of Inlet Temperature and Pressure Distortion on Turbojet Performance," NASA, Washington, DC, Report No. TM-X-71431.

[7] Biesiadny, T. J., Klann, G. A., and Little, J. K., 1984, "Response of a Small-Turboshaft-Engine Compression System to Inlet Temperature Distortion," NASA, Washington, DC, Report No. TM-83765.

[8] Soeder, R. H., Mehlic, C. M., and Stancik, K., 1985, "Effect of Steady-State Temperature Distortion on Inlet Flow to a High-Bypass-Ratio Turbofan Engine," NASA, Washington, DC, Report No. TM-86896.

[9] Mehlic, C. M., 1988, "Effect of Spatial Inlet Temperature and Pressure Distortion on Turbofan Engine Stability," NASA, Washington, DC, Report No. TM-100850.

[10] Page, J. H., Hield, P., and Tucker, P. G., 2017, "Effect of Inlet Distortion Features on Transonic Fan Rotor Stall," ASME Paper No. GT2017-64612.

[11] Hall, D. K., Greitzer, E. M., and Tan, C. S., 2017, "Analysis of Fan Stage Conceptual Design Attributes for Boundary Layer Ingestion," ASME J. Turbomach., **139**(7), p. 071012.

[12] Marble, F., 1964, "Three-Dimensional Flow in Turbomachines," *High Speed Aerodynamics and Jet Propulsion*, W. R. Hawthorne, ed., Princeton University Press, Princeton, NJ, pp. 83–166.

[13] Horlock, J. H., and Marsh, H., 1971, "Flow Models in Turbomachines," IMechE J. Mech. Eng. Science, **13**(5), pp. 358–368.

[14] Horlock, J. H., 1971, "On Entropy Production in Adiabatic Flow in Turbomachines," ASME J. Basic Eng., **93**(4), pp. 587–593.

[15] Gong, Y., Tan, C. S., Gordon, K. A., and Greitzer, E. M., 1999, "A Computational Model for Short-Wavelength Stall Inception and Development in Multistage Compressors," ASME J. Turbomach., **121**(4), pp. 726–734.

[16] Peters, A., Spakovszky, Z. S., Lord, W. K., and Rose, B., 2015, "Ultrashort Nacelles for Low Fan Pressure Ratio Propulsors," ASME J. Turbomach., **137**(2), p. 021001.

[17] Defoe, J. J., and Spakovszky, Z. S., 2013, "Effects of Boundary-Layer Ingestion on the Aero-Acoustics of Transonic Fan Rotors," ASME J. Turbomach., **135**(5), p. 051013.

[18] Gunn, E. J., Tooze, S. E., Hall, C. A., and Colin, Y., 2013, "An Experimental Study of Loss Sources in a Fan Operating with Continuous Inlet Stagnation Pressure Distortion," ASME J. Turbomach., **135**(5), p. 051002.

[19] ANSYS® CFX, Release 16.2, ANSYS CFX-Solver Theory Guide, ANSYS, Inc.

[20] Pointwise®, Release 17, Pointwise User Manual, Pointwise, Inc., 2015.

[21] Daly, M., 2013, *Jane's Aero-Engines 2013/2014*, Jane's Information Group.

Table 1. Whittle Laboratory BLI fan rig design parameters

Flow coefficient, $= \dot{m}/(\overline{\rho}_1^M A_1 U_{\mathrm{mid}})$	0.5
Stage work coefficient, $= \Delta h_t / U_{\mathrm{mid}}^2$	0.47
Stage reaction	0.81
Rotor inlet tip Mach number	0.13
Rotor tip Reynolds number	2.0×10^5
Rotor inlet hub-to-tip radius ratio	0.3
Rotor inlet tip diameter	0.5 m
Number of rotor blades	20
Number of stator vanes	30

Table 2. Inlet distortion characterizations.

	Vertically stratified		Radially stratified			
	$\left(\frac{\Delta p_t}{\overline{\rho}_1^M U_{\mathrm{mid}}^2}\right)$	$\left(\frac{\delta}{2R_{\mathrm{in}}}\right)$	$\left(\frac{dp_t}{dr'}\right)\left(\frac{R_{\mathrm{in}}}{\overline{\rho}_1^M U_{\mathrm{mid}}^2}\right)$	$\left(\frac{dh_t}{dr'}\right)\left(\frac{R_{\mathrm{in}}}{U_{\mathrm{mid}}^2}\right)$	α'	$\left(\frac{\Delta R}{R_{\mathrm{in}}}\right)$
Total pressure	0.25	0.50				
(BLI)	0.50	0.25				
	0.50	0.50				
	0.50	0.75				
	0.50	1.00				
	0.75	0.50				
Total pressure			0.974			0.75
(propeller)			1.85			0.25
			1.85			0.50
			1.85			0.75
			2.81			0.75
Total temperature				0.974		0.75
(propeller)				1.85		0.25
				1.85		0.50
				1.85		0.75
				2.81		0.75
Swirl					-15.0°	0.75
(propeller)					-10.0°	0.75
					-5.3°	0.75
					5.3°	0.75
					10.0°	0.75
					15.0°	0.75
Combined			0.974	0.974		0.75
(propeller)			1.85	1.85		0.25
			1.85	1.85		0.50
			1.85	1.85		0.75
			1.85	1.85		1.00
			2.81	2.81		0.75
			0.974	0.974	-5.3°	0.75
			0.974	0.974	5.3°	0.75
			1.85	1.85	-10.0°	0.75
			1.85	1.85	10.0°	0.75
			2.81	2.81	-15.0°	0.75
			2.81	2.81	15.0°	0.75

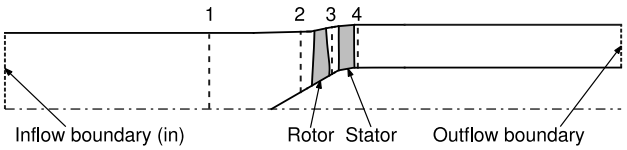

Fig. 1. Meridional view of computational domain, showing locations of measurement planes, blade rows, and inflow/outflow boundaries

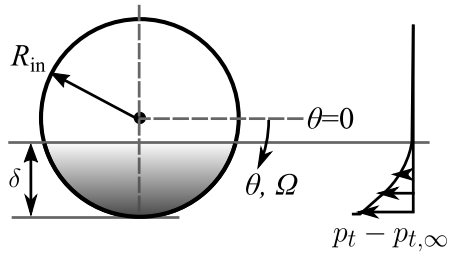

Fig. 2. Schematic illustration of vertically stratified inlet distortions of stagnation pressure.

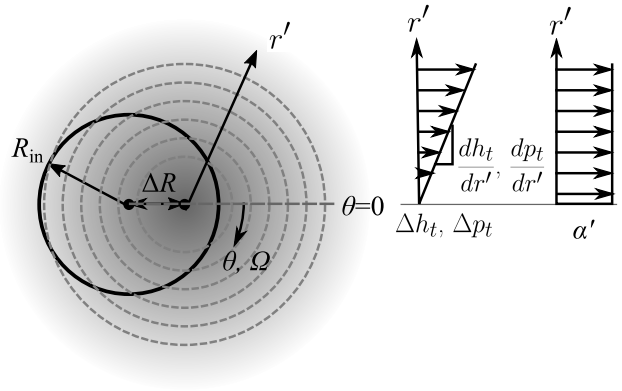

Fig. 3. Upstream propeller geometry relative to fan duct, showing h_t, p_t, and swirl (α') distributions.

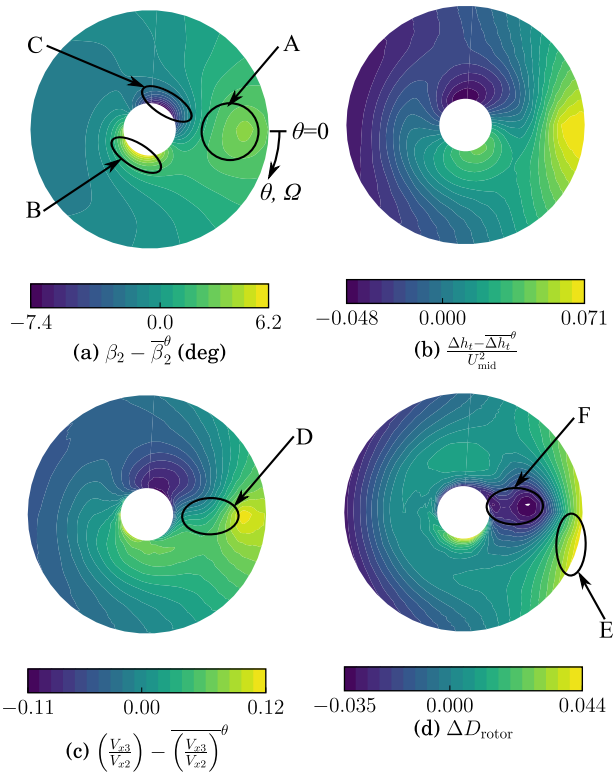

Fig. 4. Calculated rotor inlet relative flow angle distortion (a), stagnation enthalpy rise (b), streamtube contraction (c), and diffusion factor (d), for offset radially stratified inlet stagnation pressure distortion ($(dp_t/dr')\left(R_{\mathrm{in}}/\overline{\rho}_1^M U_{\mathrm{mid}}^2\right) = 1.85, \Delta R/R_{\mathrm{in}} = 0.75$).

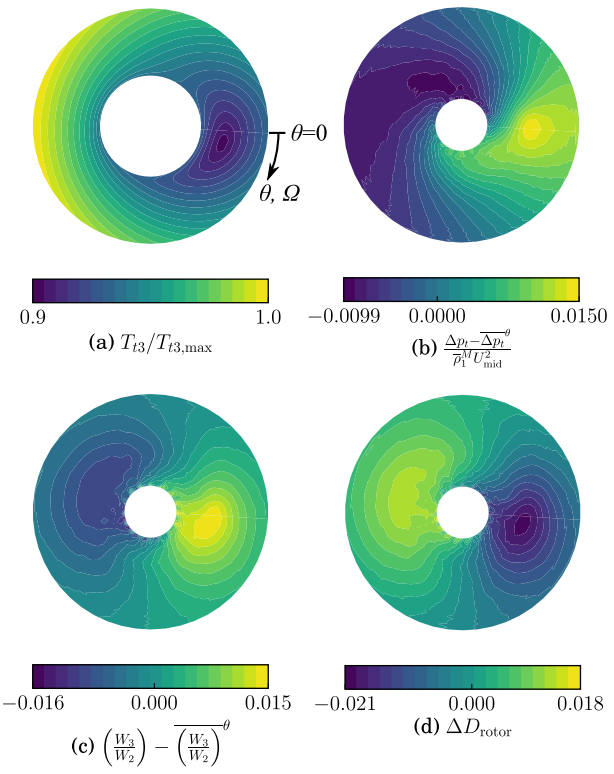

Fig. 5. Calculated stage exit stagnation temperature distribution (a), rotor stagnation pressure rise distortion (b), de Haller number distortion (c), and diffusion factor distortion (d), for radially stratified inlet stagnation temperature distortion ($(dh_t/dr')(R_{\mathrm{in}}/U_{\mathrm{mid}}^2) = 18.3$, $(\Delta R/R_{\mathrm{in}}) = 0.50$).

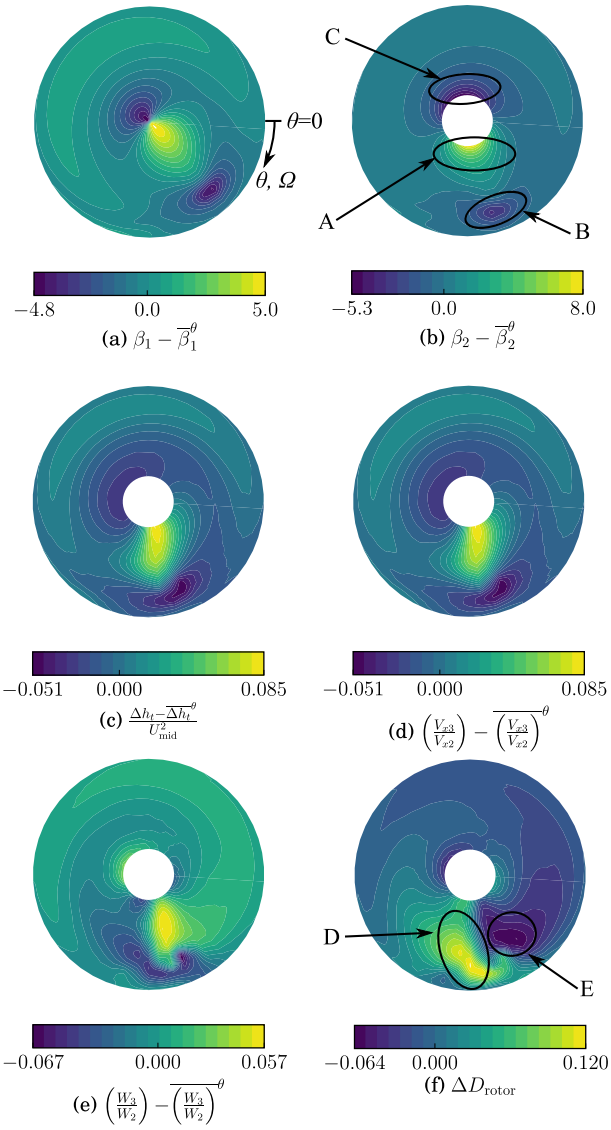

Fig. 6. Calculated rotor relative swirl angle at station 1 (a) and station 2 (b), rotor stagnation enthalpy rise distortion (c), streamtube contraction distortion (d), de Haller number distortion (e), and diffusion factor distortion (f), for radially stratified inlet swirl distortion ($\alpha' = 15°$ co-swirl, $\Delta R/R_{\text{in}} = 0.75$).

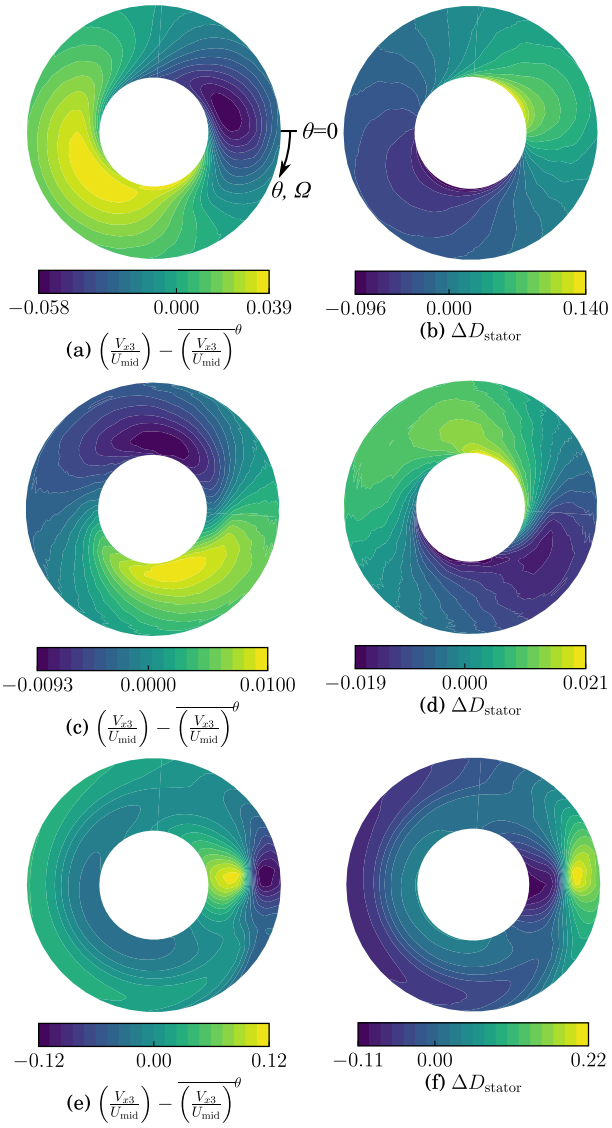

Fig. 7. Calculated rotor exit axial velocity distortion (a, c, e) and stator diffusion factor distortion (b, d, f) for radially stratified inlet stagnation pressure distortion (a and b), stagnation temperature distortion (c and d) and swirl distortion (e and f).

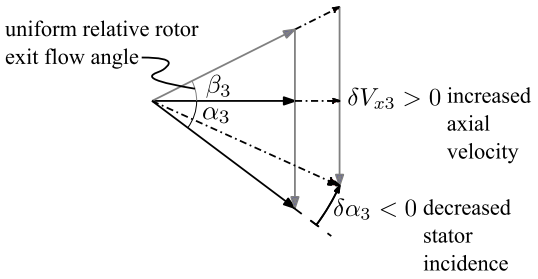

Fig. 8. Effect of varying axial velocity on stator incidence.

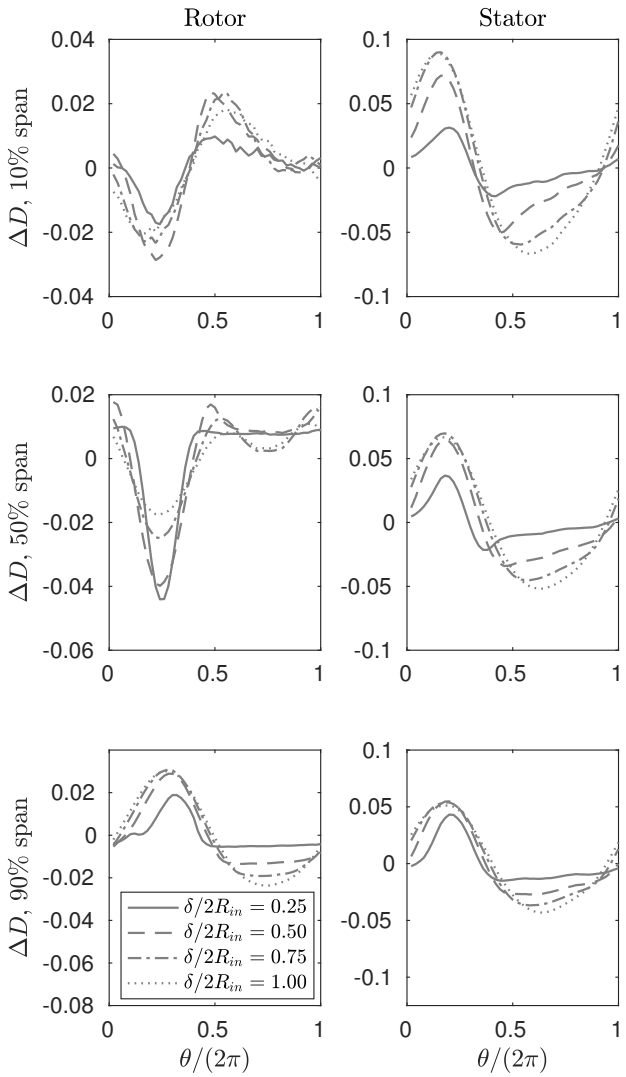

Fig. 9. Circumferential variation in rotor and stator diffusion factors at 10%, 50%, and 90% span for vertically stratified stagnation pressure distortion with $\Delta p_t/\overline{\rho}_1^M U_{\mathrm{mid}}^2 = 0.094$.

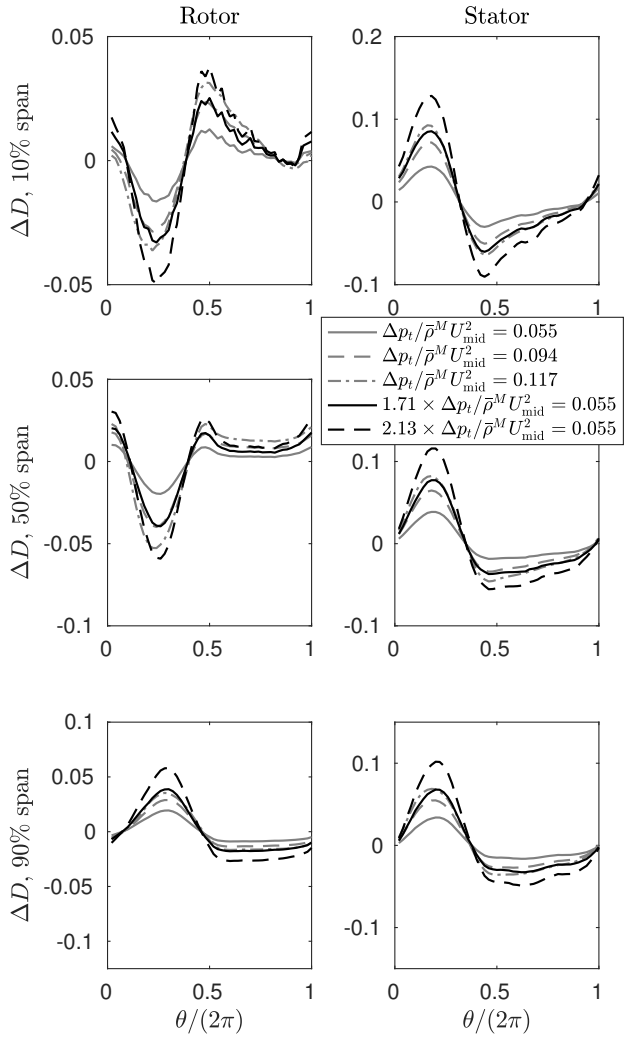

Fig. 10. Circumferential variation in rotor and stator diffusion factors at 10%, 50%, and 90% span for vertically stratified stagnation pressure distortion with $\delta/2R_{in} = 0.50$.

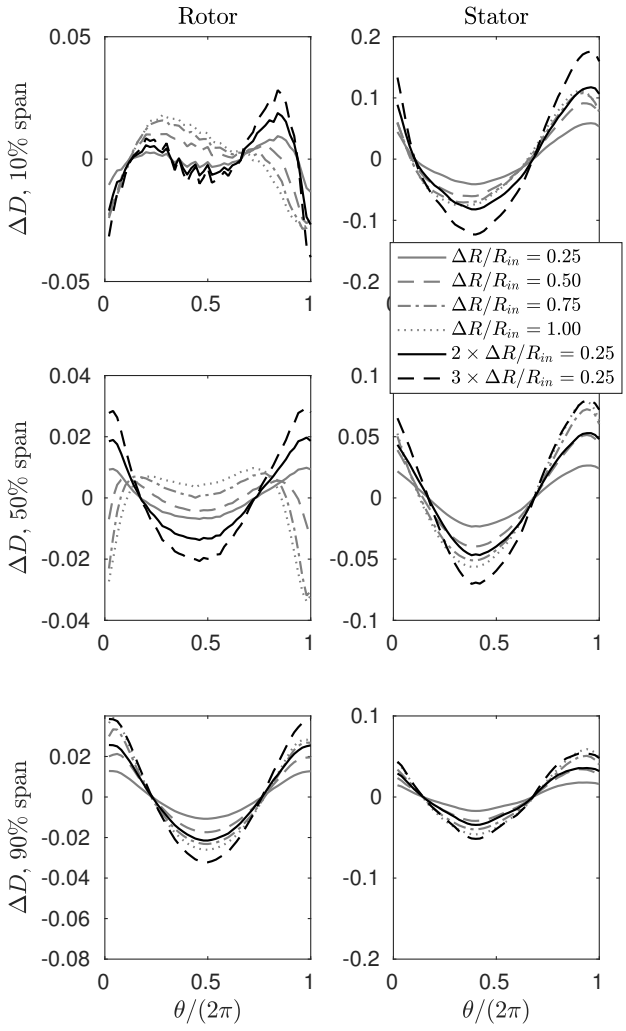

Fig. 11. Circumferential variation in rotor and stator diffusion factors at 10%, 50%, and 90% span for radially stratified distortion with $(dh_t/dr')\left(R_{\rm in}/U^2_{\rm mid}\right) = (dp_t/dr')\left(R_{\rm in}/\overline{\rho}^M_1 U^2_{\rm mid}\right) = 1.85$.

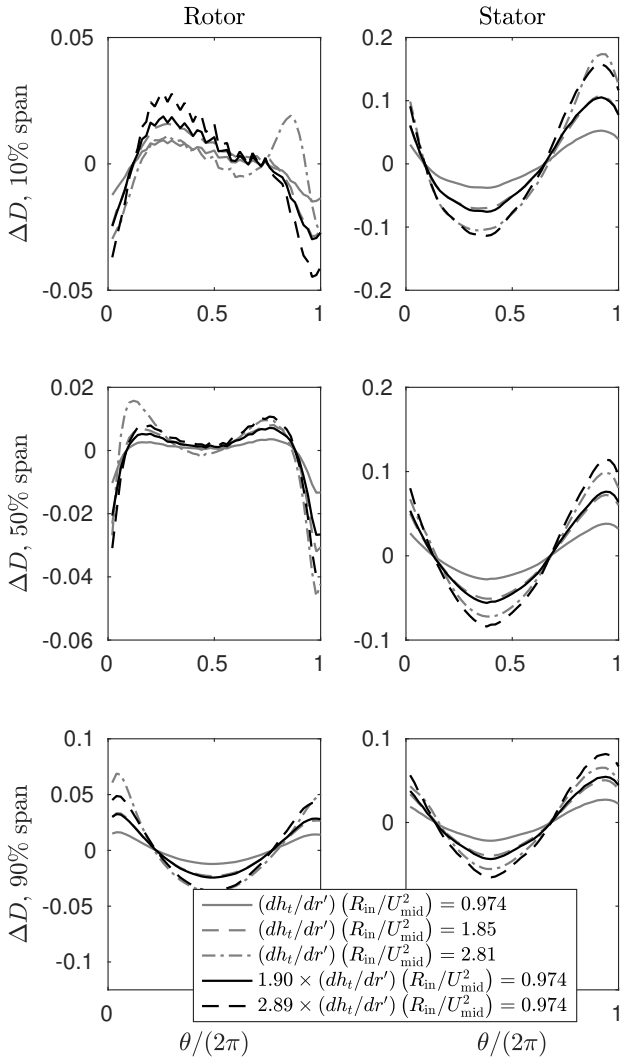

Fig. 12. Circumferential variation in rotor and stator diffusion factors at 10%, 50%, and 90% span for radially stratified distortion of p_t and h_t with $\Delta R/R_{\rm in} = 0.75$.

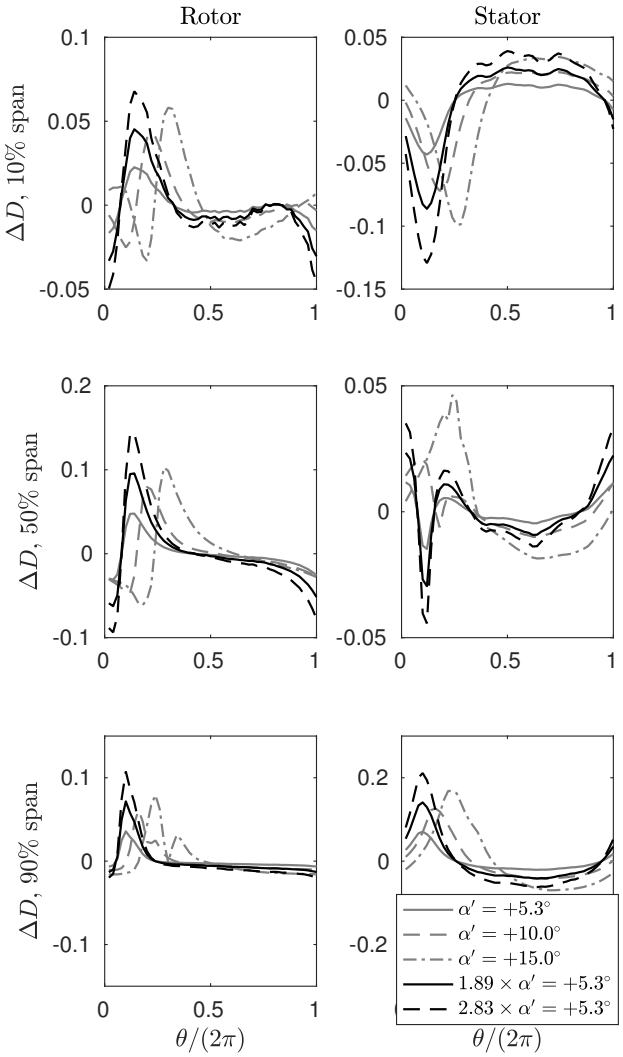

Fig. 13. Circumferential variation in rotor and stator diffusion factors at 10%, 50%, and 90% span for radially stratified co-swirl distortion with $\Delta R/R_{\text{in}} = 0.75$.

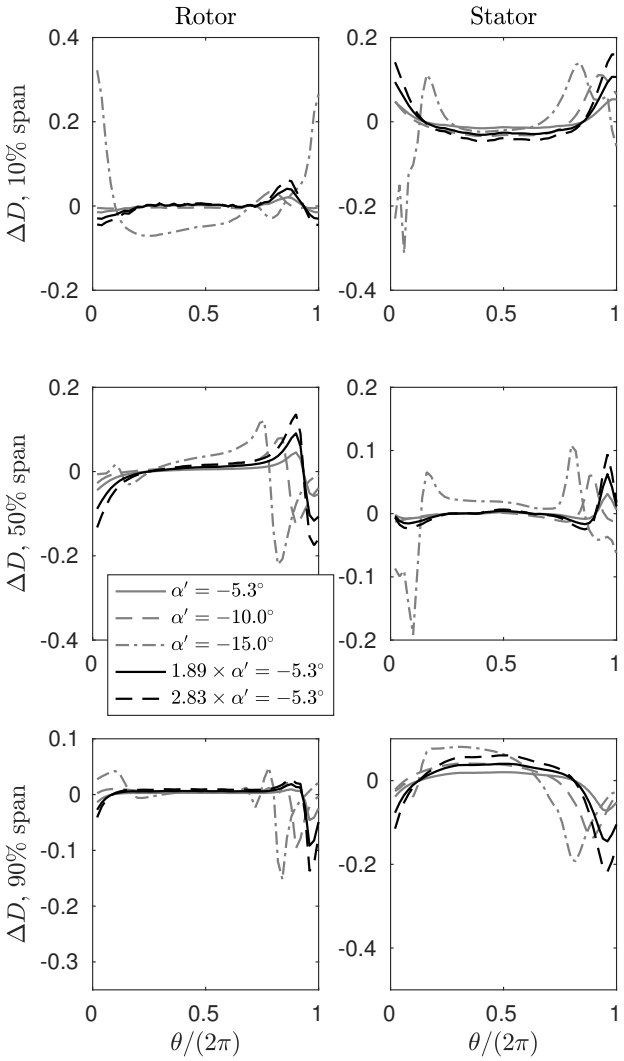

Fig. 14. Circumferential variation in rotor and stator diffusion factors at 10%, 50%, and 90% span for radially stratified counter-swirl distortion with $\Delta R/R_{\text{in}} = 0.75$.

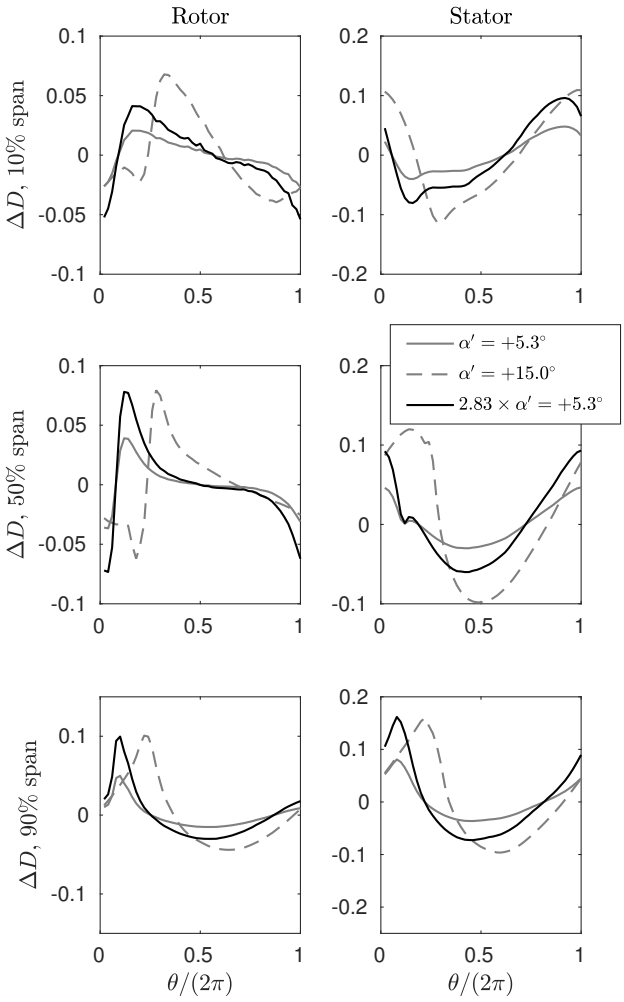

Fig. 15. Circumferential variation in rotor and stator diffusion factors at 10%, 50%, and 90% span for radially stratified co-swirl and stagnation enthalpy/pressure distortion with $\Delta R/R_{\text{in}} = 0.75$.

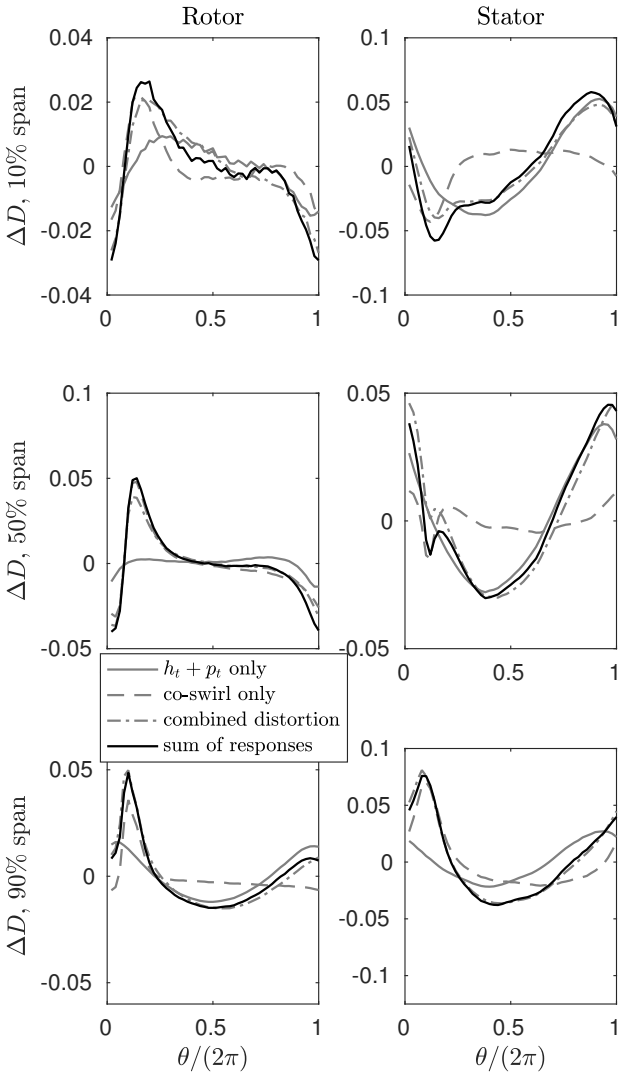

Fig. 16. Circumferential variation in rotor and stator diffusion factors at 10%, 50%, and 90% span for radially stratified co-swirl, stagnation enthalpy/pressure, and combined distortions with $\Delta R/R_{\text{in}} = 0.75$ and 5.3° co-swirl.

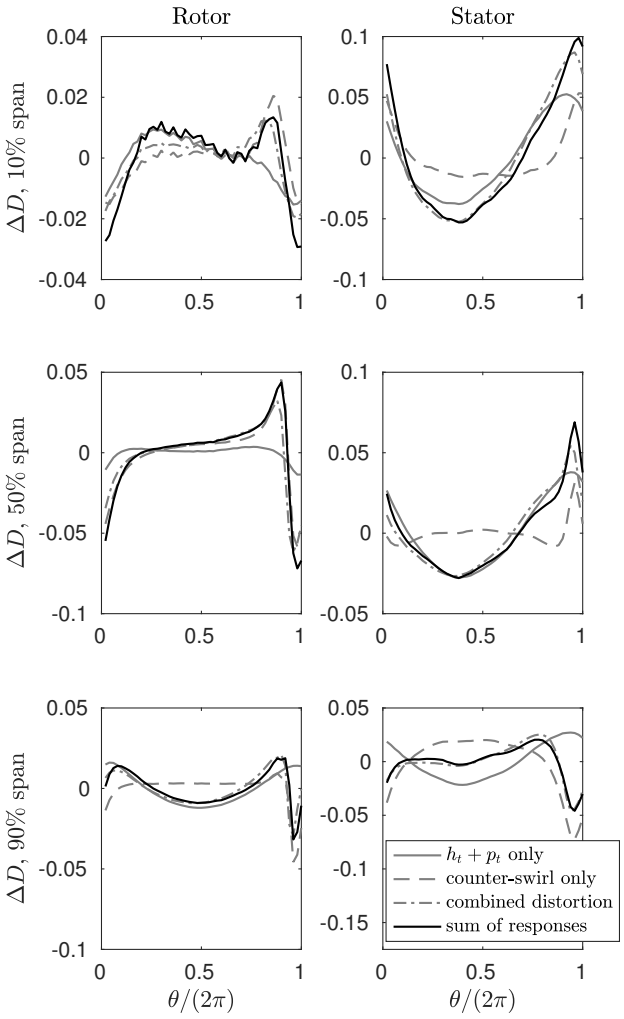

Fig. 17. Circumferential variation in rotor and stator diffusion factors at 10%, 50%, and 90% span for radially stratified counter-swirl, stagnation enthalpy/pressure, and combined distortions with $\Delta R/R_{\text{in}} = 0.75$ and 5.3° counter-swirl.